RANS Simulations of the UTSA Mach 7 Ludwieg Tube

Ian P. Bashor[1] and Christopher S. Combs[2]
The University of Texas at San Antonio, San Antonio, Texas, 78249

The University of Texas at San Antonio (UTSA) is currently constructing a high-speed wind tunnel to investigate aerodynamic phenomena at hypersonic Mach numbers, with an anticipated completion date in mid-2019. A short-duration Ludwieg tube design will be employed owing to its relatively low cost per run and ease of operation. In the current manuscript, an overview of the UTSA Mach 7 Ludwieg tube will be provided, including highlights covering the design of an appropriate converging-diverging nozzle, diaphragm system, driver tube, and other supporting devices. A commercially available CFD software package, ANSYS FLUENT, has been employed to verify the initial calculations and provide a general idea of system behavior. Reynolds-averaged Navier-Stokes (RANS) simulations of the two-dimensional flow through the nozzle, including contours of velocity magnitudes, pressures, and temperatures are presented and discussed. Key areas included are the nozzle outlet and throat section of the converging-diverging nozzle. The simulations will allow for determination of flow quality into the test section and ensure there are no shock waves generated due to the contour design. The results show that the current iteration of the nozzle contour provides a uniform velocity, temperature, and pressure profile at the outlet of the nozzle with weak expansion waves at the throat. The Mach waves quickly dissipate with distance along the nozzle and do not impede flow quality at the outlet. The expansion wave is to be expected as the nozzle design was developed by the Method of Characteristics (MOC). Upon its completion, UTSA's hypersonic Mach 7 Ludwieg tube will provide UTSA faculty and students with a high-speed test platform to investigate hypersonic phenomena including shock-wave/boundary-layer interactions (SWBLI), corner flows, complex jet-in-crossflow interactions, and hypersonic boundary layer physics while providing users experience with non-intrusive measurement techniques and laser diagnostics.

Nomenclature

T_o	=	Total Temperature in Driver Tube
P_o	=	Total Pressure in Driver Tube
$T_{Test\ Section}$	=	Static Temperature in Test Section
$P_{Test\ Section}$	=	Static Pressure in Test Section
$V_{Test\ Section}$	=	Velocity in Test Section
y^+	=	Dimensionless Distance from Nozzle Wall
ρ	=	Density
u_τ	=	Velocity in Line with Nozzle Centerline
y	=	Distance from Nozzle Wall
μ	=	Viscosity of Fluid

---

[1] Graduate Research Assistant, Department of Mechanical Engineering, AIAA Student Member.
[2] Dee Howard Endowed Assistant Professor, Department of Mechanical Engineering, AIAA Member.

I. Introduction

The University of Texas at San Antonio (UTSA) is currently constructing a high-speed wind tunnel to investigate aerodynamic phenomena at hypersonic Mach numbers, with an anticipated completion date in mid-2019. A short-duration Ludwieg tube design will be employed owing to its relatively low cost per run and ease of operation. [1] Other advantages of a Ludwieg tube facility include the ability to operate with a relatively small compressed gas reservoir (typically just the driver tube) and a simpler heating arrangement for high Mach number testing compared to conventional blow-down facilities, as the stagnant gas can simply be pre-heated prior to a test. However, as opposed to a blow-down wind tunnel with relatively long run times on the order of minutes, a short-duration Ludwieg tube design operates with run times on the scale of milliseconds.[2] Relatively short test times place an emphasis on high-speed data acquisition and instrumentation so that statistically significant data sets can be collected.**Error! Bookmark not defined.** Since this type of facility requires a high-pressure reservoir with a smaller volume than a blow-down tunnel, Ludwieg tube facilities can often be operated with a variety of test gases.

There are several supersonic wind tunnel facilities across the world that employ a Ludwieg tube design. Cummings and McLaughlin[2] and Lindorfer et al.[3] both provided thorough reviews of existing Ludwieg tube wind tunnels in 2012 and 2016. Both papers introduce facilities such as the Boeing/AFOSR Quiet Tunnel at Purdue University, a facility capable of Mach 6 flow with a 241mm (9.5 inch) diameter test section.[1] The Ludwieg tube at the California Institute of Technology (Caltech) can operate at Mach 2.3 or 4 with a test section area of 200 mm × 200 mm.[4] There are also Ludwieg tube facilities at the University of Southern Queensland[5] and throughout Germany,[6-8] the Netherlands,[9] Russia, Romania, South Korea,[10] Saudi Arabia, and the USA.[11,12] The Air Force Research Laboratory (AFRL)[13] recently developed a Ludwieg tube capable of producing flow at Mach 6. This wind tunnel employs a fast acting valve instead of a traditional diaphragm to trigger the start of a test run. Lindorfer et al. also discuss the three proposed Ludwieg tube facilities that the University of Tennessee Space Institute (UTSI) plans to construct that will range from Mach 4-7 (the 24 in × 24 in Mach 4 facility is currently operational). Other Ludwieg tubes recently developed in academia over the past couple of years are those developed by the University of Oxford,[14] University of Notre Dame,[15] University of Maryland,[16] and the University of Arizona.[17] The Oxford High Density Tunnel (HDT) utilizes a fast acting plug valve similar to that utilized by the AFRL tunnel and is designed for variable Mach numbers ranging from three to seven with a 760mm test diameter (29.92 in). The Notre Dame Ludwieg tube is designed as a Mach 6 quiet tunnel similar to that at Purdue University. One notable difference is that the Notre Dame tunnel will utilize a fast acting valve instead of a diaphragm rupture to trigger the start of a test run. The test section of the tunnel will be 1.07 m in diameter (42 in). The University of Maryland facilities will take advantage of the Ludwieg tube design with isentropic compression heating in which the compression of the fluid in the high pressure driver tube will result in sufficient fluid heating instead of external heating systems. This facility will be designed to run at Mach 6 flows. Finally, the Arizona wind tunnel is designed to run at Mach flows between 1.5 and 5. This design is an open inlet design with ambient conditions and the pressure ratio required for higher Mach numbers is provided by a vacuum chamber on the exhaust side of the diffuser. The test section for the Arizona tunnel measures 120 mm × 76.2 mm (4.72 in × 3 in).

In this paper, the design of the UTSA Mach 7 Ludwieg tube will be discussed with an emphasis on computational analysis. A commercially available CFD software package, ANSYS Fluent, has been employed to verify the initial calculations and provide a general idea of system behavior. Upon its completion, UTSA's hypersonic Mach 7 Ludwieg tube will provide UTSA faculty and students with a high-speed test platform to investigate hypersonic phenomena including, but not limited to, shock-wave/boundary-layer interactions (SWBLI), corner flows, complex jet-in-crossflow interactions, and hypersonic boundary layer physics while providing users experience with non-intrusive measurement techniques and laser diagnostics.

II. Theory

The design of high-speed wind tunnels has been well documented in the existing literature base with supersonic and hypersonic designs dating back to the 1940's.[18,19] The basic design of a Ludwieg tube consists of a high pressure driver tube filled with compressed gas followed by a diaphragm or fast-response valve. The valve or diaphragm separates the high-pressure test gas from the nozzle, test section, diffuser, and vacuum tank. Once the valve opens or the diaphragm bursts, the high-pressure test gas exhausts through the nozzle and into the vacuum dump tank, producing supersonic flow (M>1). The overall design at UTSA borrows from the extensive experience of the aerothermodynamic testing community, implementing features employed in many previous Ludwieg tube designs. Noteworthy is the design employed by AFRL including the folded driver tube that is used to conserve space while increasing the driver tube length (and thus steady-state test time).[13] A conceptual diagram of the design to be employed at UTSA can be viewed in Figure 1.
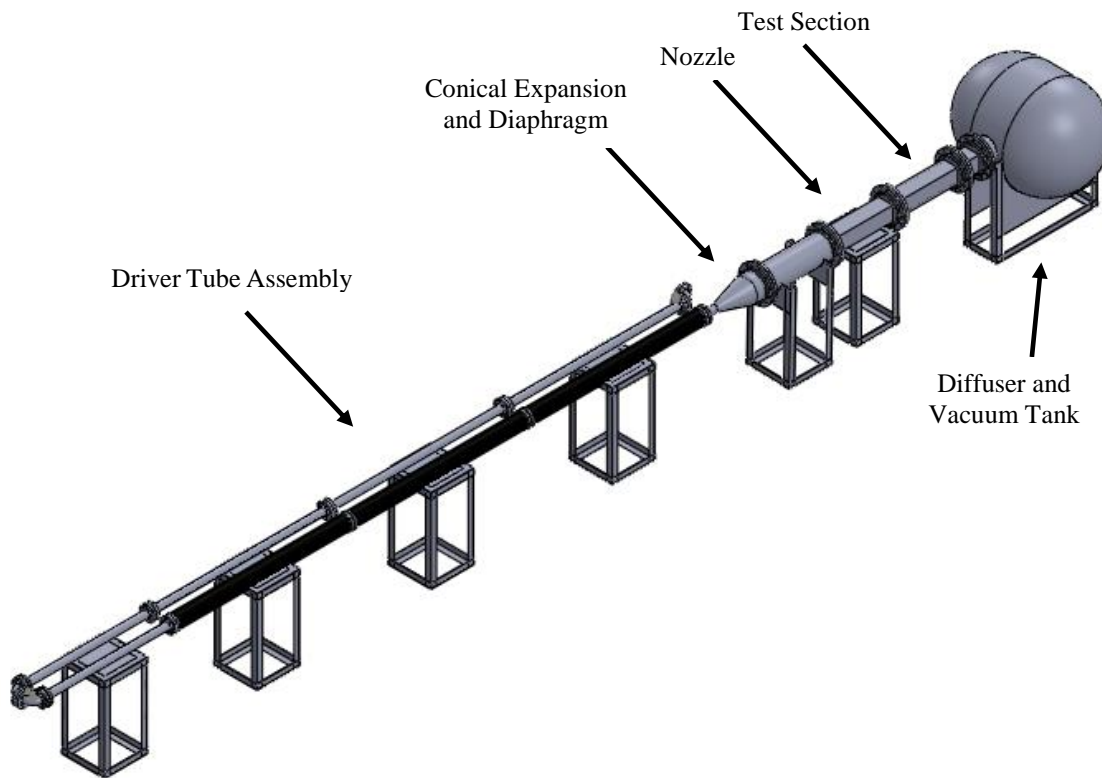
Figure 1: Conceptual Layout of UTSA Hypersonic Ludwieg Tube

Figure 1 shows all of the major components of the facility excluding the compressor and vacuum pump. The last third of the driver tube is shown covered in insulation for heating of the gas that will travel through the test section during a single wind tunnel run, consisting of multiple passes under steady state conditions. Despite the short run time, steady state assumptions are valid, as test articles will experience several hundred to several thousand flow lengths (depending on test article size) in the UTSA facility.

After diaphragm rupture, the driver tube will produce an expansion wave that will propagate from the diaphragm back through the driver tube. This expansion wave will travel through the driver tube at the speed of sound, reflect off the end of the driver tube, and reflect back to the diaphragm. Individual wind tunnel test runs will be defined by the periods of time that steady state conditions are produced in the wind tunnel test section, which will occur while the expansion wave is traveling though the driver tube. A step in flow conditions will occur when the expansion wave reaches the test section. Due to this relationship, the time of a single test is directly proportional to the length of the driver tube.**Error! Bookmark not defined.**

After the expansion wave has traveled the distance of the driver tube the pressure will drop in a step-wise manner and the process will repeat itself until the pressure difference across the nozzle drops below the required pressure gradient necessary to sustain supersonic flow.[3] With the Ludwieg tube facility it is possible to experience multiple passes of steady state conditions depending on driver tube and vacuum tank sizes and initial pressures. The number of passes is a function of the test time duration (length of driver tube), mass flow rate (nozzle design of Mach number), and vacuum tank reservoir (tank size).

The analytical analysis of the proposed wind tunnel was performed in guidance with Anderson's Modern Compressible Flow text and is assumed to be a quasi-one-dimensional flow.[19] Other assumptions are an adiabatic system, neglecting friction, inviscid fluid, and an ideal gas of air. Table 1 shows the design criteria of key parameters throughout the wind tunnel. The information under the Design Parameters include the desired characteristics of the wind tunnel that were assumed for calculations. The Mach number was chosen to be well into the hypersonic regime, the vacuum tank size was limited due to cost and physical dimension size, and the driver tube was also limited by the physical constraints of the testing facilities.

Table 1: Key Parameters of UTSA's Mach 7 Wind Tunnel

Design Parameters		Calculated Values	
Design Mach Number	7	$T_{Test\ Section}$	64.82 °K
Test Section Cross-Section	0.20m x 0.20m (8in x 8in)	$P_{Test\ Section}$	3.33 kPa (0.48 psia)
Vacuum Tank	6.06 (m^3)	$V_{Test\ Section}$	1,129 m/s
T_o	700 K	Mass Flow Rate	8.36 kg/s
P_o	13.79 Mpa (2000 psia)	Time of Test	70 ms
Diffuser Efficiency	45%	Reynolds Number	$47 \times 10^6\,\mathrm{m^{-1}}$
Driver Tube Length	18.29m (60ft)	Mach Number in Driver Tube	0.044
		Number of Steady State Passes	4
		Driver Tube	4 in nominal (3.44in I.D.)

III. Experimental Method

ANSYS CFX was first utilized for the initial iterations of the Mach 7 nozzle and facilities but due to the limited node count on the academic license ANSYS Fluent was pursued instead. This was because external resources to UTSA were accessible with node counts greater than the 500k limit. The geometry was imported as an external step file that was originally created in SolidWorks. The text file that defined the contour was built from the Method of Characteristics (MOC). The FORTRAN code utilized for this process was shared with UTSA by Dr. Rodney Bowersox (Texas A&M) who is the original developer. Several frozen bodies were added in the throat region of the nozzle to assist in the meshing portion as a region of influence where the mesh needed further refinement.
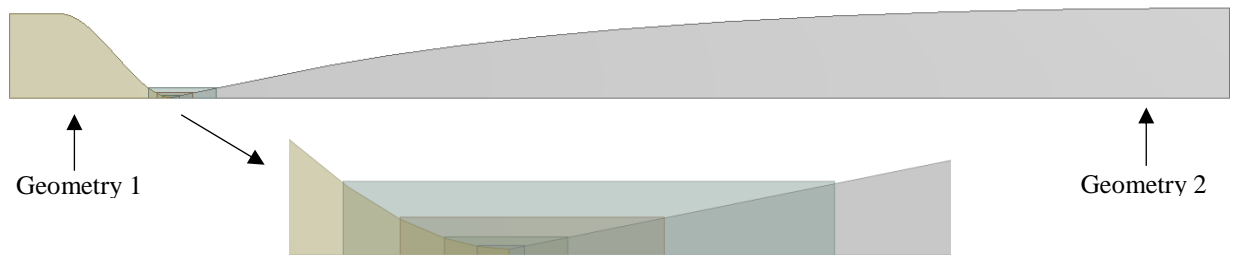

Figure 2: Example Geometry with Bodies of Influence

Figure 2 shows the bodies of influence that were added in the geometry and that the diverging and converging portion of the nozzle were imported as two separate geometry files. This was done to create two separate domains that could be initialized to separate conditions.

The mesh was created utilizing a general body sizing, edge sizing at the upper wall, and body sizings for the three regions of influence. The edge sizing was critical to develop the correct y^+ values at the wall for the turbulent model that was selected in the solution initialization. The y^+ value is a dimensionless measurement of distance normal to a wall in fluid flow. This parameter is critical to ensuring resolution of viscous models employed in the boundary layer of the flow. The general form of y^+ can be found in Eq. (1).

$$y^+ = \frac{\rho\, u_\tau\, y}{\mu} \qquad \text{Eq. (1)}$$

A bonded contact was created between the diverging and converging domains so the contact region could be manipulated in the solution initialization. Figure 3 shows the mesh methodology that was utilized for the nozzle contour.
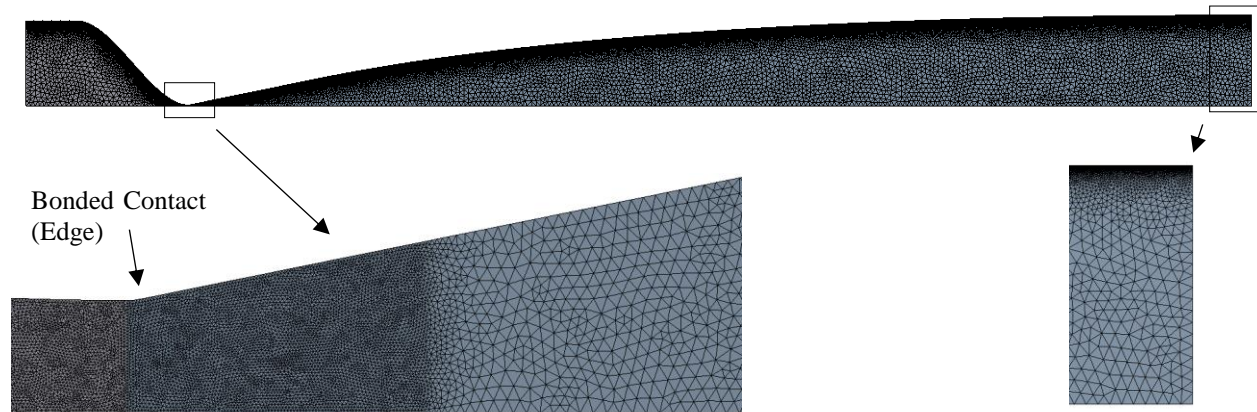

Figure 3: Mesh of Nozzle

In Figure 3, it is possible to see the mesh refinement in the throat and the edge sizing. The bonded region between the converging and diverging geometry is also shown. As this is a 2-D example case the contact regions are the touching edges. In a 3-D geometry this would be defined as the touching faces.

A density based solver was chosen due to the compressible nature of the fluid. The fluid density for air was changed to an ideal gas and the energy model was turned on. The turbulent model chosen was the k-ω SST model with viscous heating and compressibility effects.

Table 2: Boundary Condition Summary

Boundary Condition	Quantity	Set Parameters
Interior	3	---
Inlet	1	Pressure Inlet @ 13.79 MPa and 700°K
Outlet	1	Pressure Outlet @ 3.33 kPa and 64°K
Symmetry	2	---
Wall	3	Stationary and No Slip

In Table 2 the boundary conditions are summarized. The inlet and outlet conditions match that of the given conditions in Table 1. The pressure outlet would hold the pressure constant until local Mach numbers of 1 or greater were achieved. After the flow is locally supersonic only upstream pressures and temperatures are referenced at the boundary condition.[20] Next the flow was initialized to the pressure and temperatures per the analytical model shown in Table 1. Monitors of the static temperature, pressure, and Mach number were set in the diverging portion of the nozzle. Mass flow in and out were also monitored for steady state convergence. The mesh between the converging and diverging portions of the nozzle were fused together to make a smooth mesh transition between the two domains. Finally the y+ adaption feature of Fluent was utilized to compute and adapt the mesh at the wall based on mean stream conditions. On the 2-D cases the y+ was adapted to a value under ten. Finally, an implicit second-order upwind scheme was utilized for spatial discretization. A Courant number of 0.1 was specified as the initial iterations needed a relatively small value to assist with convergence. Initially, residual values of 1×10^{-6} were targeted, however, the residuals plateaued on the order of 1×10^{-5} and convergence was never reached. The output residuals in ANSYS Fluent are

normalized to the peak values within the first 5 iterations. For the absolute residuals the final residuals need to be multiplied by the peak residual value within the first 5 iterations.

IV. Results

The simulations were run for an array of tests and the results are presented in chronological order. The first test that was completed was for the nozzle only with a 0.19 m (7.5 in) height inlet. Figure 4 shows the density gradient of the throat area to highlight the expansion waves from the MOC design. It was also discovered that there was a shock wave that was forming. The density gradient was viewed as a representative view of how Schlieren imaging would look in the contour of the nozzle. As a common method for viewing shock and expansion waves in the test section of the tunnel it gives a good idea of what is to be expected during experimentation.
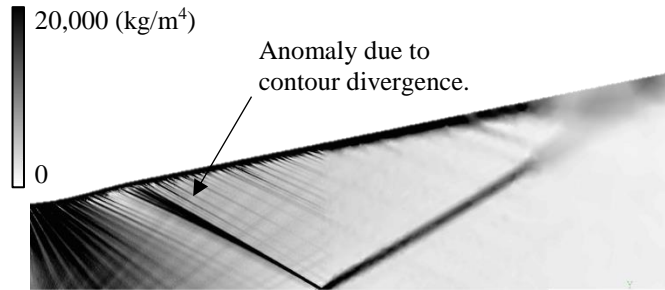

Figure 4: Density Gradient of Throat Area

Oblique shock calculations showed that this feature was a weak shock-wave with a flow turning angle of 0.8° with Table 3 showing the upstream and downstream properties. The shock was a result of an anomaly on the contour of the nozzle wall which resulted in a negative turning angle. A new nozzle contour was developed to correct the anomaly and hence removed the shock.

Table 3: Properties Across Shock

	Upstream	Downstream	
Velocity	765.3	758.5	(m/s)
Pressure	2.095	2.190	MPa
Temperature	409	414.2	K
Mach Number	1.89	1.86	

Figure 5 shows the same graph as Figure 4, however, the anomaly in the throat has been resolved and the mesh has been increased along the edge of the contour and in the throat region. The increased mesh had a value of 527k nodes while the reduced mesh was on the order of 350k nodes. Boundary conditions, initialization, and computational schemes were held constant across simulations.

Figure 5: Density Gradient of Throat Area Updated Contour

The dark region in the throat area shows the expansion fan through the throat region and shows the absence of the shock wave from the previous contour. The initial dark region on the far left of the figure shows the initial expansion fans but it is also possible to see the wave reflections immediately downstream of the turning angle. Figure 6 shows the full contour of the diverging nozzle with the density gradient plotted as would be viewed in Schlieren imaging. The full contour shows that the flow quality has little to no variance in the mean free-stream density at the nozzle exit.

Figure 6: Full Contour of Density Gradients

In Figure 6 it's possible to see the boundary layer grow in the diverging part of the nozzle. The boundary layer growth can be observed by the dark region that propagates down from the nozzle wall. The lighter region above the almost black region at the nozzle exit means that the density gradient is less severe and the boundary layer is becoming well developed. The boundary layer is measured at 0.01m (0.57 in) thick at the nozzle outlet. Other properties of interest were the static temperature, pressure, and velocity of the flow through the contour as well as at the outlet of the nozzle. Figure 7 shows the pressure contour of the nozzle.
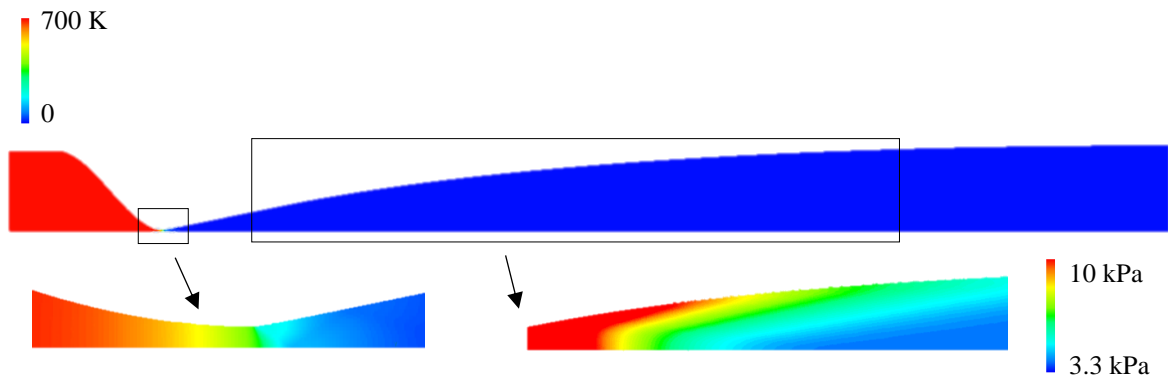

Figure 7: Pressure Contour

Special areas of interest are shown in Figure 7 consisting of the throat and nozzle exit. The throat is important as it would also identify shock waves as the density gradient does and would be observable here. However, the detailed view of the throat area shows a smooth transition from 13.8MPa (red) to 3.3 kPa (blue) as is expected from the calculations shown in Table 1.
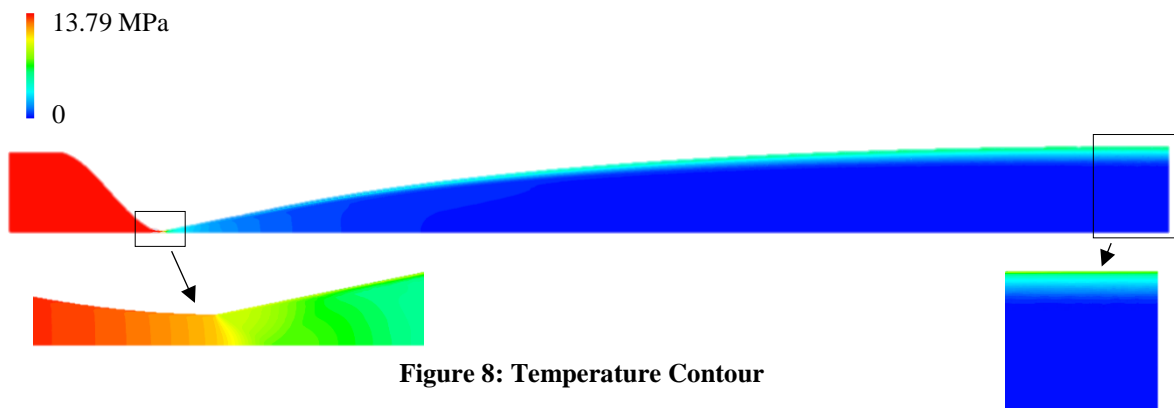

Figure 8: Temperature Contour

Figure 8 shows the temperature contour through the nozzle with the throat and nozzle exit having detail views shown. The temperature change is smooth and continuous through the throat into the diverting portion of the nozzle from 700 K (red) to 64 K (blue).
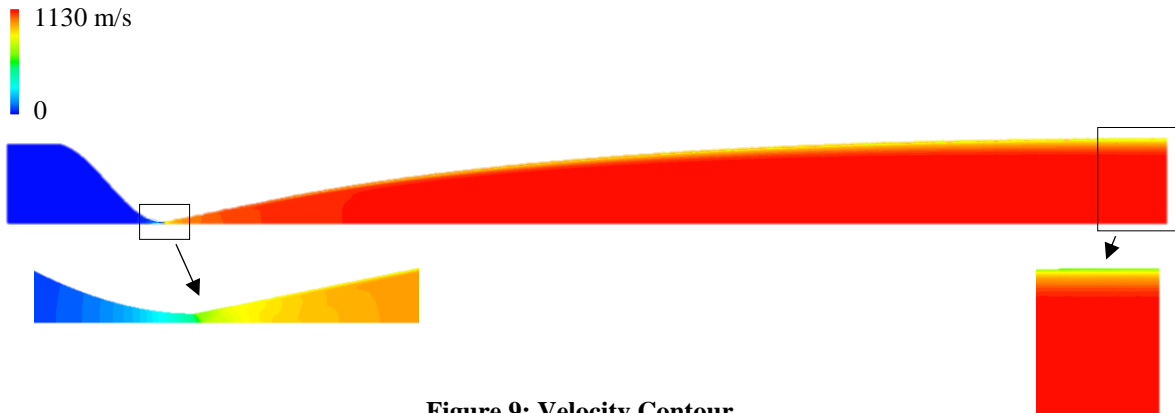

Figure 9: Velocity Contour

Figure 9 shows the velocity contour of the overall nozzle, throat, and outlet. The velocity reaches values close to those outline in Table 1 and the outlet velocity is plotted on a graph to get an estimate of the boundary layer thickness leading into the test section. The Prandtl number is the ratio of viscous diffusion rate to the thermal diffusion rate. This means that the thermal and momentum boundary layers will not grow at the same rate with nozzle distance. The ratio of the thermal and momentum boundary layer thicknesses should by definition be equal to the Prandtl number. The ratio of the momentum boundary layer thickness to the thermal boundary layer thickness was found to be 0.74 at 99% of the freestream values, which is equal to the Prandtl number of air at the simulated flow conditions. From Figure 10 it was determined that the maximum velocity at the outlet was 1130 m/s. Looking at 95% of the mean flow as the boundary layer, this velocity occurs at 1.48×10^{-2} m from the top of the nozzle (0.58 in).

Next the Mach number contour is shown in Figure 10. The Mach number contour is a function of the pressure, temperature, and velocity contours. Here it is possible to see the transition from subsonic to supersonic flow in the throat as well as the boundary layer at the exit of the nozzle. A graph of the nozzle exit is show in Figure 11.
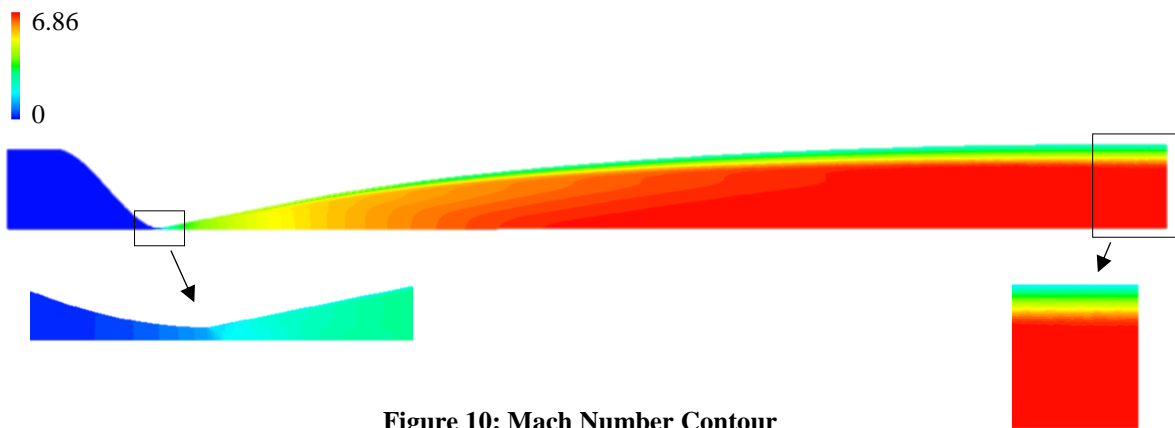

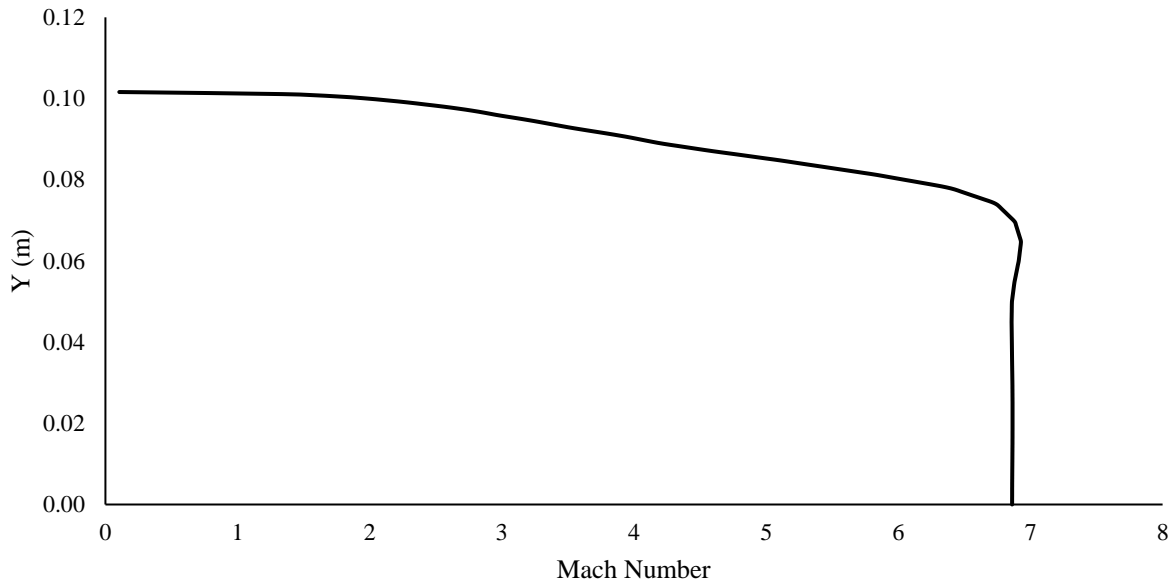
Figure 10: Mach Number Contour

American Institute of Aeronautics and Astronautics

Figure 11: Mach Number at Outlet

Figure 11 shows that there is a slight spike in the Mach number between the free stream flow and the boundary layer. As the mean flow is steady and close to the design value of seven it shows good flow quality leaving the nozzle and entering the test section where it achieves a value of 6.86. The Mach number and Y distance was then normalized and compared to the data presented in Lindorfer et al. paper and their Mach number was estimated along the normalized Y and then normalized to the max value.
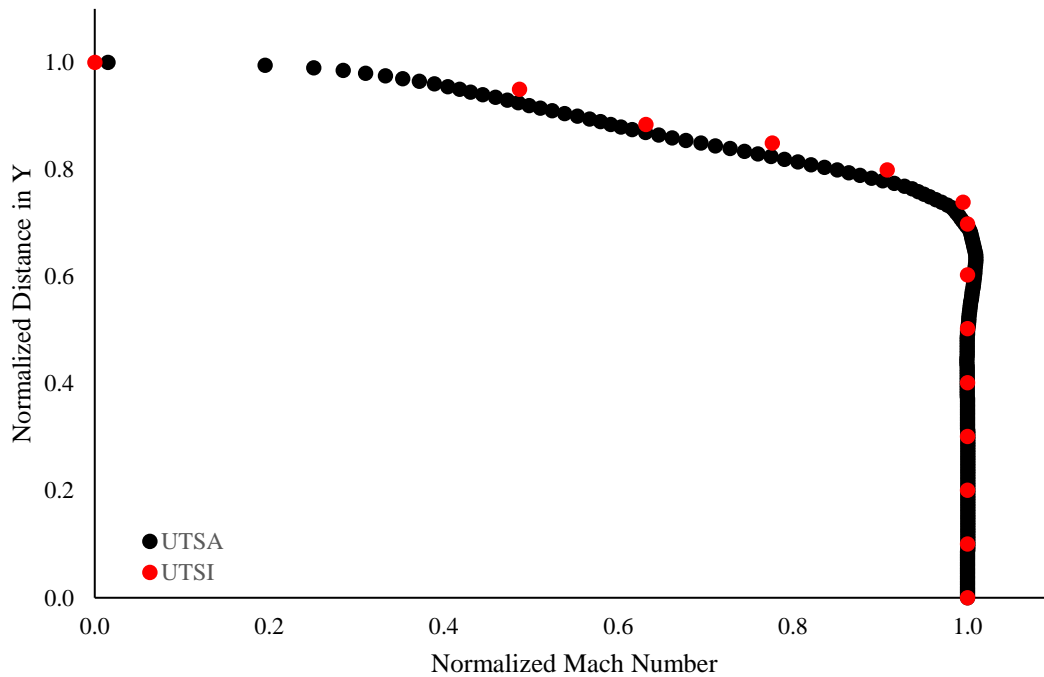

Figure 12: Normalized UTSA Mach number data compared to Lindorfer, et al. published Mach number data[3]

American Institute of Aeronautics and Astronautics

V. Conclusion

In conclusion, the 2-D SS solution was utilized to verify the nozzle contour of the UTSA Ludwieg tube wind tunnel and avoid any potential shock generation. A weak shock was found in the initial contour design and then removed in the following contour iteration. The density gradient was viewed as a representative view of how Schlieren imaging would look in the contour of the nozzle. As a common method for viewing shock and expansion waves in the test section of the tunnel it gives a good idea of what is to be expected during experimentation. Furthermore, the Mach number contour shown in Figure 11 closely resembles the normalized Mach number profiles published by Lindorfer et al. in their analysis of the UTSI Mach 4 wind tunnel.[3] This is verified in Figure 12.

The boundary layer height will be taken into account during selection of model size. The gradient of density, shown in Figure 6, shows that the flow quality into the test section in the free stream remains constant outside of the boundary layer. This will provide uniform velocity, pressure, and temperature profiles normal to the contour wall in the free stream at the nozzle outlet. The free stream properties found from the simulation were found to be a Mach number of 6.84, 70.97 K, 1126 m/s, and 3,749 Pa which compare well with the calculated values of 7, 64 K, 1130 m/s, and 3330 Pa. The Prandtl number was calculated at 0.74 at the 99% boundary layer and by definition is the ratio of the momentum boundary layer height to that of the thermal boundary layer.

While the results of these initial simulations are promising there is much room for future work. The current nozzle design could be simulated in three-dimensional space and the cross sectional area out of the nozzle should be analyzed to take into account additional fluid phenomena arising from corner flow effects. A transient analysis of both the current 2-D case and 3-D model would allow for time sensitive data to be analyzed and transient effects on the first pass and subsequent passes to be identified.

American Institute of Aeronautics and Astronautics

Acknowledgments

References

[1] Schneider, Steven, and Craig Skoch. "Mean flow and noise measurements in the Purdue Mach-6 quiet-flow Ludwieg tube." *15th AIAA Computational Fluid Dynamics Conference*. 2001.

[2] Cummings, R. M., & McLaughlin, T. E., "Hypersonic Ludwieg Tube Design and Future Usage at the US Air Force Academy" *50th AIAA Aerospace Sciences Meeting including the New Horizons Forum and Aerospace Exposition*. Nashville, TN. 2012

[3] Lindorfer, S. A., Anusonti-Inthra, P., Combs, C. S., Kreth, P. A., & Schmisseur, J. D., "An Investigation of the Role of an Upstream Burst Diaphragm on Flow Quality within a Ludwieg tube using RANS" *46th AIAA Fluid Dynamics Conference*. Washington, D.C., 2016

[4] El-Naggar, M. Y., Klamo, J. T., Tan, M. H., & Hornung, H. G., "Experimental Verification of the Mach-Number Field in a Supersonic Ludwieg Tube" *AIAA Journal*, Vol. 42, No. 8, 2004, pp. 1721-1724.

[5] Buttsworth, D., "Ludwieg Tunnel Facility with Free Piston Compression Heating for Supersonic and Hypersonic Testing" *Proceedings of the 9th Australian Space Science Conference*. Sydney, AU. 2009. (pp. 153-162).

[6] Estorf, Malte, Wolf, Torsten, and Radespiel, Rolf, "Experimental and Numerical Investigations on the Operation of the Hypersonic Ludwieg Tube Braunschweig". *Proceedings of the Fifth European Symposium on Aerothermodynamics for Space Vehicles*, Cologne, Germany. 2005

[7] Juhany, K. A., and Aldakhil, H., "AT0 Ludwieg Tube Wind Tunnel at KAU," AIAA Paper 2006-1316, Jan. 2006.

[8] Friehmelt, H., Koppenwallner, G., and Müller-Eigner, R., "Calibration and First Results of a Redesigned Ludwieg Expansion Tube," AIAA Paper 93-5001, Dec. 1993.

[9] Schrijer, F. F. J., and Bannink, W. J., "Description and Flow Assessment of the Delft Hypersonic Ludwieg Tube," Journal of Spacecraft and Rockets, Vol. 47, No. 1, Feb. 2010, pp. 125-133.

[10] K. David, J. Gorham, S. Kim, P. Miller, and C. Minkus, "Aeronautical Wind Tunnels: Europe and Asia," Library of Congress Research Report, Feb. 2006.

[11] M. Holden, K. Chadwick, and J. Kolly, "Hypervelocity Studies in the LENS Facility," AIAA Paper 95-6040, April 1995.

[12] T.P. Wadhams, E. Mundy, M.G. MacLean, and M.S. Holden, "Experimental and Analytical Studies of Transition in High Speed Flows at CUBRC," AIAA Paper 2008-4395, June 2008.

[13] Kimmel, R. L., & Borg, M., "AFRL Ludwieg Tube Initial Performance" *55th AIAA Aerospace Sciences Meeting*. Grapevine, TX. 2017.

[14] McGilvray, M., Doherty, L. J., Neely, A. J., Pearce, R., & Ireland, P. (2015). The Oxford High Density Tunnel. In 20th AIAA International Space Planes and Hypersonic Systems and Technologies Conference (p. 3548).

[15] Lakebrink, Matthew T., Kevin G. Bowcutt, Troy Winfree, Christopher C. Huffman, and Thomas J. Juliano. "Optimization of a Mach-6 Quiet Wind-Tunnel Nozzle." Journal of Spacecraft and Rockets 55, no. 2 (2017): 315-321.

[16] Chung, Joseph, and Stuart J. Laurence. "Adiabatic-compression preheated Ludwieg tube for the realistic simulation of hypersonic flows." In 20th AIAA International Space Planes and Hypersonic Systems and Technologies Conference, p. 3547. 2015.

[17] Threadgill, James A., Ilona Stab, Adam Doehrmann, and Jesse C. Little. "Three-dimensional flow features of swept impinging oblique shock/boundary-layer interactions." In 55th AIAA Aerospace Sciences Meeting, p. 0759. 2017.

[18] Pope, Alan., and Goin, Kennith L., *High Speed Wind Tunnel Testing*, Huntington, New York, 1978, Chaps. 1, 2, 4, 11.

[19] Anderson, John, D. Jr., *Modern Compressible Flow*, New York, New York, 1982, Chaps. 1, 2, 3, 4, 5.

[20] Fluent, Inc. "FLUENT user's guide." Lebanon, NH2007 (2006).